applied sciences

MDPI

Article

Mechanical and Microstructural Studies of High Performance Concrete with Condensed Silica Fume

Piotr Smarzewski

Faculty of Civil Engineering and Geodesy, Military University of Technology, 2 Gen. Sylwestra Kaliskiego, 00-908 Warsaw, Poland; piotr.smarzewski@wat.edu.pl; Tel.: +48-69-869-5284

Abstract: This article is an extended version of the conference paper "Influence of silica fume on mechanical and fracture properties of high performance concrete" published in Procedia Structural Integrity as a part of the Special Issue for the 3rd International Conference on Structural Integrity (ICSI 2019). Tests were carried out to evaluate the compressive strength, tensile splitting strength, modulus of elasticity, flexural strength, and fracture properties of high performance concretes (HPC) having different levels of condensed silica fume (CSF) replacements for cement. It was found that CSF replacement for cement by up to 25% may have a favorable effect on the mechanical properties. HPC containing CSF was characterized by quite large increases in compressive strength (up to 14%) and flexural strength (16%). However, the most significant improvements in mechanical properties were obtained for splitting tensile strength (26%) and fracture energy (30.5%). There were slight reductions up to 2% in the elastic modulus, flexural strength and fracture properties at the 25% level of CSF substitution for cement. Microstructural studies showed that the narrowest microcracks and the smallest pores in the interfacial transition zone (ITZ) between the paste and grains of aggregate occurred in the HPC having 10% CSF. In addition, a reduction of ITZ around the aggregate and the formation of more high-strength hydration products was observed in all CSF-added HPCs. The outcomes reported that CSF can successfully replace cement. It is suggested that the substitution should not exceed 20%.

Keywords: high performance concrete; condensed silica fume; compressive strength; tensile splitting strength; elastic modulus; fracture properties; microstructural properties

Citation: Smarzewski, P. Mechanical and Microstructural Studies of High Performance Concrete with Condensed Silica Fume. *Appl. Sci.* **2023**, *13*, 2510. https://doi.org/10.3390/app13042510

Academic Editor: Jong Wan Hu

Received: 5 January 2023
Revised: 8 February 2023
Accepted: 14 February 2023
Published: 15 February 2023

1. Introduction

High performance concrete (HPC) is a concrete based on a cement matrix with natural aggregate and added additives and admixtures, which is distinguished by, among others, good workability for at least 1 h, compressive strength over 60 MPa at 28 days, and water/binder ratio less than 0.4. In order to obtain a tighter structure of the mixture, micro-fillers and nanoparticles are used, e.g., fly ash, silica fume, ground granulated blast furnace slag, metakaolin, and nano-silica [1–10]. Compared to normal strength concrete, HPC has a more homogeneous and dense structure with a smaller number of pores and shrinkage cracks occurring. For example, HPC with compressive strength of not more than 90 MPa can be easily manufactured by using moderate amounts of ordinary aggregate, silica fume, and a superplasticizer [11].

HPC is applicable to many civil engineering structures, including skyscrapers and bridges. Its use may result in the lowering of the construction costs, causing a visible reduction in the cross-sections of concrete structures [12]. This may be advantageous in columns in terms of the benefits of long span requests and reducing the consumption of steel reinforcement [13]. Although HPC is stiffer and more durable than normal strength concrete, it also has greater brittleness, which may make it more susceptible to cracking and brittle failure [14]. The high ductility of HPC may be reached by proper selection of the kind and grain size of the aggregate [15,16] or the use of fibers [17–21].

Interest in the application of silica fume began with strict control of air pollution. In numerous countries, industrial plants have been forced to stop releasing silica fume into the atmosphere by using special devices for its accumulation. After the tests, it was stated that the collected silica fume can be used as an addition of a reactive binder in concrete [22].

Silica fume is an industrial by-product mainly produced during the manufacturing of ferro-silicon. It is formed by the decomposition of high purity quartz with coal or else coke and wood shavings in an electric arc furnace throughout the fall of metallic silicon or alloy of ferrosilicon. The percentage of silicon dioxide (SiO_2) in silica fume largely depends on the type of product manufactured. The higher the production of silicon alloy, the smaller the amount of silica fume. Most of the silica fumes used are at least 75% ferro-silicon alloys [22]. Silica fume is a very fine amorphous substance and is recycled in concrete as a mineral additive with significant pozzolanic activity. To a large extent, the properties of silica fume depend on the type of product produced and the process of its production. The silica fume generally contains more than 90% SiO_2. Nevertheless, the SiO_2 content and the amorphousness degree can differ greatly depending on the production technique. Silica fume originates in three forms: powder, slurry, and condensed silica fume (CSF). The use of silica fume powder is quite problematic, as the loose bulk density ranges from 130 to 430 kg/m^3 compared to 500–700 kg/m^3 for CSF. Due to the very fine particles of the silica fume powder and its low loose bulk density, handling problems can also occur. Other problems associated with the use of this type of silica fume are its stickiness, clogging during transport, and bridging in the storage silo. The solution to the above-mentioned problems is the use of slurried silica fume or condensed silica fume (CSF). In this study, it was decided to use the latter. One method of producing CSF is to blow compressed air from the silos bottom filled with silica powder. As a result of agglomeration, the heavier particles fall to the bottom of the silo and are from time to time removed. Another method of producing CSF is the mechanical pressing of silica fume powder. The earliest example of the use of silica fumes is a 15% cement substitution in the tunnel construction in Norway [22].

CSF impacts the HPC in twofold, key ways. Firstly, CSF acting a part to the reaction of hydration between water and cement by reacting with the hydroxide of calcium to form a gel of calcium silicate hydrate (CSH), which is the binder between the aggregate grains and provides the mechanical strength of HPC. What is more, the ultra-fineness constituent part of CSF (<1 μm) occupies the holes between the particles of cement, consequently acting as a micro-filler, reducing the cement porosity [23]. This results in lower permeability and better HPC durability. However, the homogeneous dispersion of CSF in HPC can be problematic. The heterogeneity can be caused by the influence of ball bearing as well as local problems. Thus, heterogeneity in the structure of pores may cause serious durability issues [22]. From some perspectives, CSF is a very favorable mineral supplement mainly for the production of high and ultra-high performance concrete, but caution must be taken through mixing to obtain appropriate particles' dispersion. In addition, CSF can accelerate the setting time by around 60% [24]. As a consequence, the compressive strength, tensile strength, bonding strength, freeze–thaw resistance, chemical attack resistance, and abrasion resistance of HPC showed significant improvement [25–29]. It is worth mentioning that CSF increases the concrete performance, but its efficiency is reduced when high doses of CSF or small amounts of water are used to complete pozzolanic reactions [30]. Notably, the effect of CSF filling is more leading than its pozzolanic influence. The greatest recognized impact of CSF on HPC is the enhancement of aggregate grain—cement paste interface [31–33]. CSF increases the HPC's request of water due to its ultra-fineness and direct addition. Therefore, CSF is used in a composition with a superplasticizer in order to control workability. However, investigators revealed some shortcomings associated with its use in HPC, i.e., the plasticity reduction throughout the manufacture and an increase in shrinkage during maturation [23,33].

Wedding and Swamy [34], as well as John and Shah [35] reported that experimental relations between compressive strength and physical properties, for instance elastic modulus, flexural strength, and split tensile strength, approved for normal concrete, should

not be used for HPC. Ahmad and Shah [36] stated that the crack is better localized and resembles homogenous material behavior for HPC, but the matrix is more brittle compared to normal strength concrete. Sabir [13] studied the mechanical assets of high performance CSF concrete maturated in water at 20 °C and 50 °C with cement replacement by CSF in the range of 12–28%. The results obtained at 20 °C showed that the compressive and splitting tensile strengths reduced when the CSF addition was augmented from 16% to 20%. However, the problem was not evident to samples maturated at 50 °C. The results also showed that there was no noteworthy effect on the relation between compressive and splitting tensile strength. Moreover, the tensile strength was in the range of 4–6% of the compressive strength value. In addition, compressive strengths above 90 MPa were related to decreases in elastic modulus, especially when the CSF replacement was greater than 16%. Kadri et al. [37] observed a maximum 28-day concrete strength ranging from 5 to 20% CSF replacement with cement. Gesoglu et al. [38] reported an average increase in compressive and splitting strength of about 10% in ultra-high performance cementitious mixtures with the addition of different doses of CSF and nanosilica ranging from 0.5 to 3%. Li et al. [39] highlighted that a mixture of CSF and nanosilica has a greater influence on the sulfate resistance of concrete compared to separately addition. Researchers also take issue about the optimal CSF addition [17,40] to obtain the best performance of HPC. For some of them, the CSF replacement is approximately 15% [11], while for others, the increase in mechanical characteristics can be reached from 30% to 40% of the CSF [41]. Pedro et al. [4] indicated that 10% CSF is considered ideal. Nevertheless, the cement portion can be substituted by CSF, making at least equivalent performance to HPC, reducing the CO_2 footprint.

In recent years, researchers have considered the influence of CSF on HPC performance, and their results indicate that the mechanical assets and durability of HPC are greatly improved when CSF is added. Despite the large amount of data on HPC, the current knowledge on the HPC fracture properties development with CSF content, which is beneficial for the safety of concrete structures, is still insufficient. This topic has been discussed in investigations by Kjellsen et al. [14], Zhou at al. [15], as well as John and Shah [35]. Over the past several decades, various types of fibers have been applied to increase the flexural toughness as well as crack resistance of HPC [42–45].

Fracture characteristics are very essential for durability and safety of HPC. Though, little information is currently available regarding the effect of SiO_2 microparticles on HPC fracture properties.

This article is an extended version of the conference paper "Influence of silica fume on mechanical and fracture properties of high performance concrete" published in Procedia Structural Integrity as a part of the Special Issue of the 3rd International Conference on Structural Integrity (ICSI 2019) [23]. In this work, the effects of CSF on the compressive strength and fracture characteristics of HPC with CSF addition from 5% to 25% were investigated. The water to binder ratio (W/B) was 0.25. HPC samples were also examined to determine elastic modulus and splitting tensile strength. The results are given at 28 days after water curing at 20 °C. In order to observe the effect of CSF on fracture characteristics of HPC, the mid-span deflection, stress intensity factor, elastic-plastic failure parameter, fracture energy, crack mouth opening displacement (CMOD), crack tip opening displacement (CTOD), and characteristic length of HPC notched beam specimens containing CSF were determined. Moreover, research was conducted to study the impact of CSF on the macro- and microstructural development of HPC.

2. Materials and Methods

The cement was CEM I 52.5R meeting the PN-B-19707:2013-10 [46] and PN-EN 197-1:2012 [47] standards. Tables 1 and 2 list the physical characteristics and costs, as well as chemical arrangement of condensed silica fume (CSF) and cement, respectively. It can be seen that the replacement of Portland cement CEM I 52.5R by CSF was economically and environmentally justified. Meyer [1] found that although condensed silica fume is difficult to handle due to extreme fineness, its advantages, i.e., improving the strength

and durability of high performance concrete, are so obvious that it is available not only as a by-product, but also produced specifically for the concrete industry. Quartz sand with a grain size of 0.125/0.5 mm was used as fine aggregate (FA), as well as granodiorite with 0.5/8 mm grain size was applied as coarse aggregate (CA). Size gradations of fine and coarse aggregates (quartz sand and granodiorite) were determined with the PN-EN 933-1:2012 [48] standard agreement (see Figure 1). In HPC, a light yellow color superplasticizer CX ISOFLEX 793 (CEMEX Admixtures GmbH, Salzkotten, Germany) was used, with a density of 1.07 ± 0.02 g/cm^3 and PH of 6 ± 1 at 20 °C, with alkali and chloride content below 1.5% and 0.1%, respectively, and based on polycarboxylate ethers. It was added as a percentage of the binder content.

Table 1. Physical properties and costs of cement and CSF.

Material Properties	Cement	CSF
Specific surface area (m^2/kg)	484	17,000
Water demand (%)	30	-
Start of setting (min)	160	-
End of setting (min)	210	-
Volume stability according to Le Chatelier (mm)	0	-
Compressive strength at 2 days (MPa)	40.3	-
Tensile strength at 2 days (MPa)	6.46	-
Costs (EUR/ton)	255	117

Table 2. Chemical arrangement of cement and CSF.

Composition (%)	SiO_2	Al_2O_3	Fe_2O_3	CaO	MgO	SO_3	K_2O	Na_2O	Cl	Loss on Ignition	Insoluble Matter
Cement	19.99	4.19	3.76	64.82	1.14	3.25	0.46	0.24	0.07	3.01	0.18
CSF	94.80	1.30	0.83	0.56	0.71	-	1.26	0.41	-	0.12	-

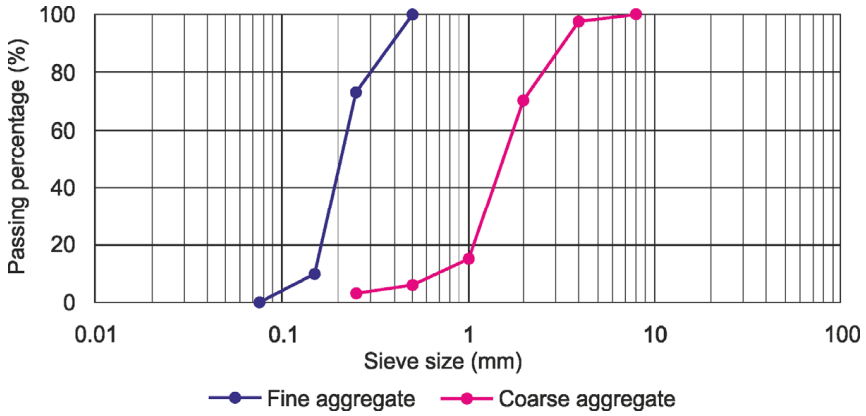

Figure 1. Particle size distribution of aggregates.

The water to binder ratio was determined based on the total amount of binder components in the mixes. The percentage of CSF was defined as the mass ratio of silica fume to cement used in the control mix.

Based on the knowledge obtained in preliminary tests, it was found that with the superplasticizer addition, it is possible to produce HPC with good workability with a maximum CSF content of 25% and W/B = 0.25. The amounts used in the reference mixture were as follows: cement—745 kg/m^3, coarse aggregate (CA)—1000 kg/m^3, fine aggregate (FA)—500 kg/m^3, superplasticizer—20 kg/m^3, and water—186 kg/m^3. The CSF mixtures were designed based on a control HPC with different cement substitutions with CSF. Table 3 displays the HPC mixtures details used in this investigation.

Table 3. Mixture proportions of HPCs.

Mixture ID	Cement (kg/m^3)	CSF (kg/m^3)	CSF (%)	CA (kg/m^3)	FA (kg/m^3)	Superplasticizer (kg/m^3)	Superplasticizer (%)	Water (kg/m^3)
CSF0	745	0	0	1000	500	20	2.7	186
CSF5	708	37	5					
CSF10	670	75	10					
CSF15	633	112	15					
CSF20	596	149	20					
CSF25	559	186	25					

Each HPC mixture was prepared in about 8 min. Mixing was finished when a homogenous blend was obtained. Cubic samples with dimensions of 100 mm × 100 mm × 100 mm were made for compressive and tensile strength examinations. Cylinders with a diameter 150 mm × height 300 mm were produced for the elastic modulus experiment, and 80 mm × 150 mm × 700 mm prismatic specimens with a mid-span notch were made for the three-point bending test. Cylinders and cubic samples were formed in plastic molds. In turn, prisms were prepared in wooden forms. Molds filled with the HPC blend were compacted on a vibrating table. The specimens were then removed from the molds after 48 h and maturated for 24 days in water at 20 °C, and after removal from the water tank in air conditions for 2 days for testing at 28 day. Three specimens were made for each blend per the respective test. Dimensions and specimens' number are specified in Table 4.

Table 4. Specimen specification.

Test	Shape	Dimensions (mm)	Number
Compression	Cube	100 × 100 × 100	18
Splitting tensile			18
Modulus of elasticity	Cylinder	150 × 300	18
Three point bending	Notched beam	80 × 150 × 700	18

3. Results and Discussion

3.1. Compressive Strength

The capacity of HPC to carry compressive loads till failure is known as compressive strength. The tests were carried out taking into account the recommendations of the PN-EN 12390-3:2019-07 [49] standard in order to determine the compressive strength after 28 days. The detailed composition of the reference mixture and the five HPC mixtures with the CSF addition changing from 5 to 25% are shown in Table 3. Three cubic samples cast per each mix. The influence of the CSF content on the development of compressive strength is presented in Figure 2.

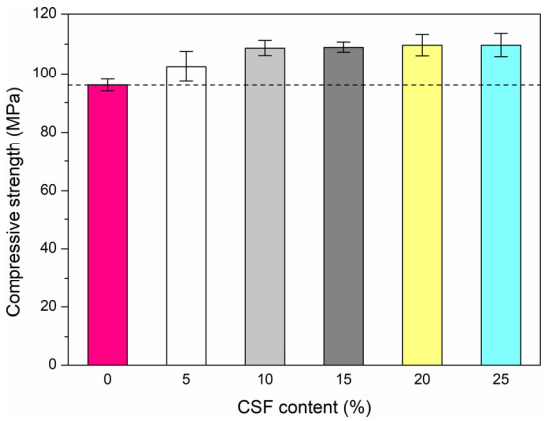

Figure 2. Differences in compressive strength with CSF substitution.

Figure 2 shows that CSF substitution with cement up to 25% can result in a noticeable enhancement in compressive strength. Increasing compressive strength in HPC has been noted with increasing CSF exchange. The increases were set at approximately 6.5%, 13%, 13.5%, 14%, and 14% for 5%, 10%, 15%, 20%, and 25% CSF replacement, respectively. The above outcomes may be influenced by the increase in the cement paste–aggregate interface bond strength caused by the filling effect of CSF. The hypothesis is supported by compression failure modes that are more explosive for CSF HPCs.

Yogendran et al. [11] examined cylinders 150 mm in diameter × 300 mm in height during compression. They reported strength increasing to 15% CSF replacement and then decreasing to 25% of the CSF used in this study. Sabir [13] reported an investigation on the compressive strength of CSF HPC at W/C = 0.35. The compressive strength after 28 days was from 74 to 110 MPa with CSF content up to 28%. Samples maturated at 20 °C with 12% and 16% CSF replacements presented a leveling of strength gain after 28 days. On the other hand, those with more than 16% CSF continued to increase compressive strength after 28 days. Moreover, the outcomes indicated that the compressive strength up to 28 days evidently decreased when the CSF content augmented in the range of 16–20%. Wu et al. [3] examined the effect of silica fume (SF) content on compressive strength of ultra-high strength concrete (UHSC). The SF content had a noteworthy influence on the compressive strength up to the 7th day of maturation. Afterwards, the increase in compressive strength was around 11%. A noteworthy increase in compressive strength was found with an increase in SF substitution in the range of 0–20%. The compressive strength tended to decrease when SF exceeded 20%. The UHPC compressive strength without SF after 28 days was 89.8 MPa. When 10%, 15%, 20%, and 25% SF substitution was employed, the compressive strength augmented by about 18%, 16%, 28%, and 25%, respectively. In the present work, it was found that the compressive strength gradually increased with increasing CSF exchange up to 20%, and then remains constant up to 25% of the applied CSF content. A similar behavior was observed by Vikan and Justnes [50], who reported that the 15–20% amount of SF improved strength and reduced porosity as a result of the pozzolanic reaction and the filling effect. They also reported that at 25% SF, yield stress as well as plastic viscosity increased, which may affect the entrapment of additional air. On the other hand, in these investigations, it was observed that HPC with 25% CSF content developed a compact and very dense matrix, as illustrated in Figure 3.

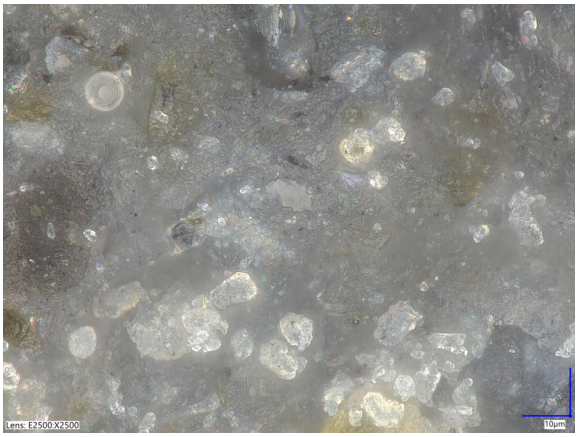

Figure 3. Dense HPC microstructure of with 25% CSF substitution.

3.2. Tensile Splitting Strength

The studies were performed according to PN-EN 12390-6:2011 [51] in order to obtain the split tensile strength of HPC. Cubic samples were aged in water at 20 °C, until examined after 28 days. Figure 4a shows the split tensile strength versus the CSF content. Strength increased as CSF replacement increased to 10%, and as CSF replacement further increased from 10% to 25%, HPC tensile strength decreased.

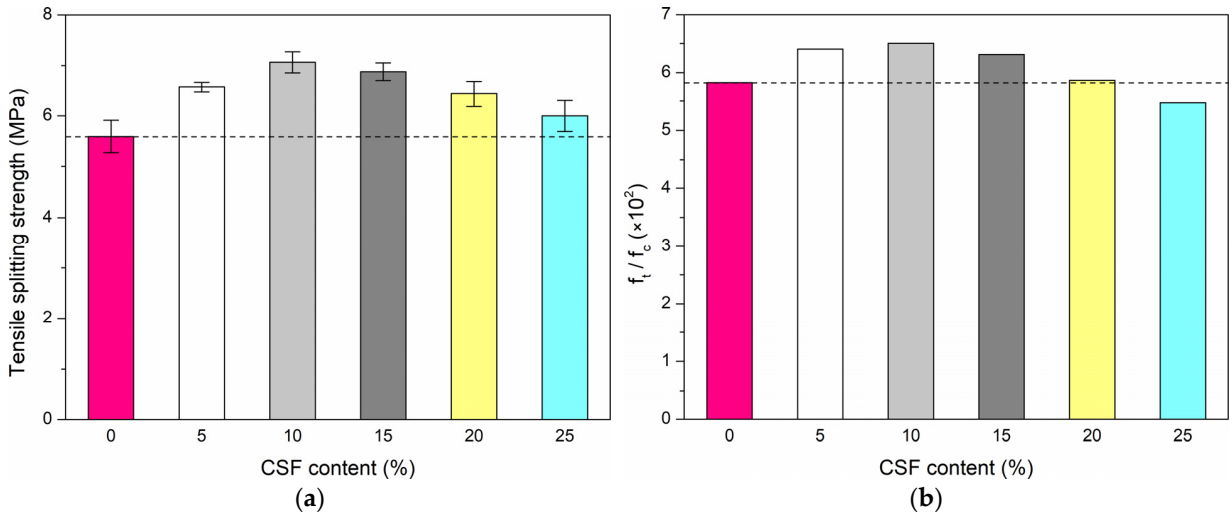

Figure 4. Differences in (**a**) tensile splitting strength; (**b**) ratio of split tensile strength to compressive with CSF replacement.

The condensed silica fume has a noticeable impact on the tensile splitting strength. 10% CSF causes an average strength increase of about 26% after 28 days. The results also designated that strength was evidently decreased with CSF replacement at the level of 20–25%, compared to 10% CSF content. A slightly different trend was reported by Sabir [13], who observed that tensile splitting strength did not increase meaningfully with growing CSF content. Similar to the compressive strength, slight reductions in tensile strength were gained when the CSF replacement was augmented at the level of 16–20%. Figure 4b presents the ratios of tensile splitting to compressive strength in relation to CSF substitution. It has been noted that growing the CSF replacement from 10% to 25% leads to a decrease in the split tensile to compressive strength ratio. On the other hand, from 0% to 10% CSF, there was a gradual increase in this ratio. This could not have been predicted, as growing CSF content usually leads to greater compressive strength, and these are related to lower ratios. Sabir [13] observed that for an increase in compressive strength in the range of 75–100 MPa, the ratio of tensile splitting strength to compressive strength falls from 6% to 4% with increasing compressive strength. This ratio initially increases from 5.8% to 6.5%, and then falls from 6.5% to 5.5% with increasing compressive strength, for compressive strengths described in this paper in the range of 96.1–109.7 MPa.

3.3. Modulus of Elasticity

The examination was conducted in accordance with ASTM C469/C469M-14 [52] to obtain the elastic modulus after 28 days. Differences in elastic modulus with CSF replacement are displayed in Figure 5.

An increase in the HPC modulus of elasticity was noted with an increase in substitution of condensed silica fume up to 10%. Additional augmented CSF replacement resulted in an increase in the amount of extra cementitious gel with a progressive decrease in the ratio of calcium-silicate. Elastic moduli of HPC were greater than modulus of elasticity of the reference HPC for CSF substitution up to 20%. The amount of gel created depended on the calcium hydroxide amount formed from the hydrated cement that could be obtained by reaction with the CSF. Thus, the additional amount of CSF did not contribute to development of elastic modulus. CSF replacement above 10% appears to have an effect on elastic moduli. The average elastic modulus increases by 5% to 10% of the CSF volume content and then falls by 5% in the range of 10–25%. Characteristic of the results obtained in this work is a slight reduction in the modulus of elasticity with the increase in compressive strength for CSF content from 10% to 25%. Sabir [13] found that a compressive strength greater than 90 MPa was associated with a significant reduction in elastic modulus. This was explained by an increase in HPC porosity above a certain critical level of CSF.

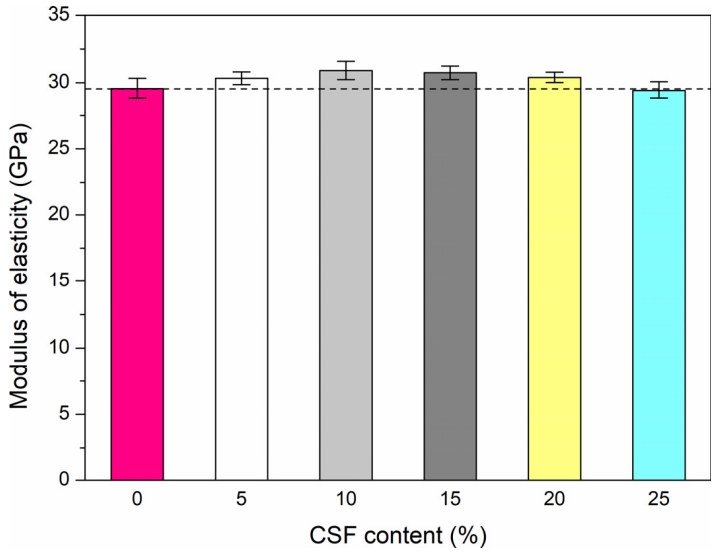

Figure 5. Variation of the elastic modulus with CSF replacement.

3.4. Flexural Strength and Fracture Properties

Prismatic specimens with notch in the center-point loading arrangement were employed in accordance with the RILEM TC 89-FMT standard [53]. Two supports were set at a distance of 600 mm. The constant rate of loading throughout the test was 0.05 mm/min. In this experiment, the flexural strength, stress intensity factor, crack mouth opening displacement (CMOD), crack tip opening displacement (CTOD), fracture energy, elastic-plastic failure parameter, and characteristic length of HPC were evaluated. In the specimen midspan, a notch was cut with a depth and thickness of 50 mm and 3 mm, respectively. Two steel sheets (see Figure 6) were then glued close to the notch to install the gauge. A linear variable displacement transducer (LVDT) installed at the midpoint of 80 × 150 × 700 mm HPC specimen was used to assess the deflection. As the experiment was conducted on the specimens, the applied load, deflection, and CMOD were automatically recorded by the data acquisition software. Representative load-deflection curves are shown in Figure 7.

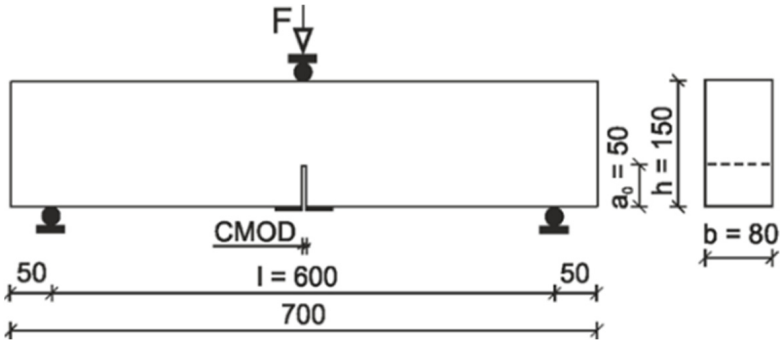

Figure 6. Geometry of notched beam specimens under center-point loading arrangement.

The response of the HPC prisms with notch in the three-point bending test was approximately linear up to the peak load. Then, the curves suddenly dropped as the prisms separated. The flexural strength and fracture properties were calculated based on Equations (1)–(8) to assess the cracking resistance of HPC beam with different CSF substitutions. The following formula was used to determine the flexural strength of the HPC prisms with notch:

$$f_{t,fl} = \frac{3F_p l}{2b(h-a_0)^2}\ (\text{MPa}) \quad (1)$$

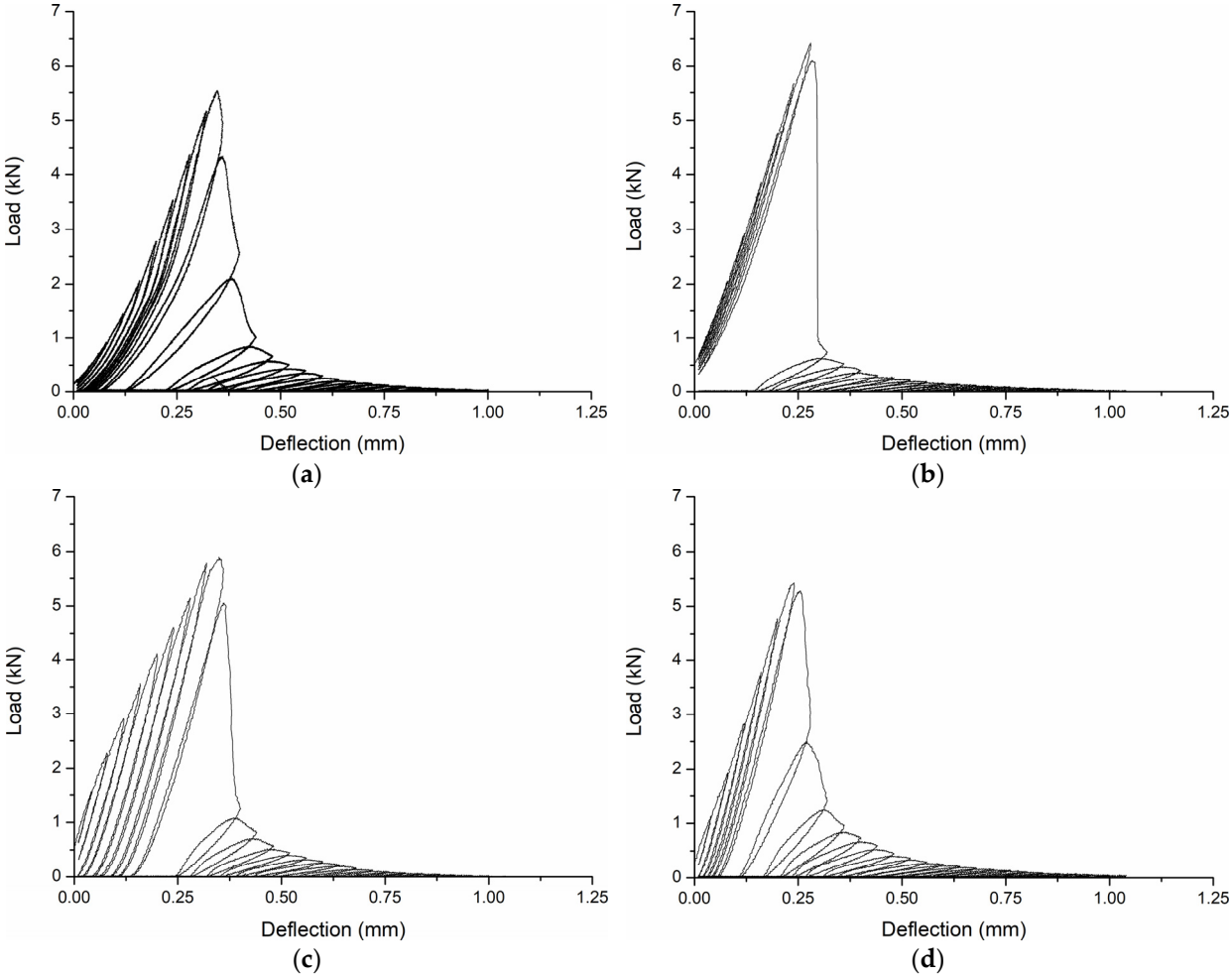

Figure 7. Exemplary test dependences of HPC load-deflection for CSF content of (**a**) 0%; (**b**) 5%; (**c**) 20%; (**d**) 25%.

The stress intensity factor K_{Ic}, representing the field of stress around the tip of the crack, was aimed at evaluating the cracking resistance of HPC prisms with various CSF substitutions on the basis of the following formula [54]:

$$K_{Ic} = \frac{F_p}{b\sqrt{h}} f(\alpha) \ (\mathrm{MN/m^{1.5}}), \tag{2}$$

where F_p is the peak load, b is the width of the prism, h is the height of the prism, and $f(\alpha)$ is a function of the sample geometry defined below:

$$f(\alpha) = 6\sqrt{\alpha}\left\{\frac{1.99 - \alpha(1-\alpha)\left(2.15 - 3.93\alpha + 2.7\alpha^2\right)}{(1+2\alpha)(1-\alpha)^{3/2}}\right\}, \tag{3}$$

where α is the relative crack length, $\alpha = a_0/h$, a_0 is the notch depth.

A higher factor (K_{Ic}) indicates that HPC has greater resistance to crack development and has enhanced fracture assets.

The fracture energy G_{Ic}, defined as the energy needed to break the specimen in load mode I, is calculated as follows:

$$G_{Ic} = \frac{{K_{Ic}}^2(1-\nu)}{E_c} \ (\mathrm{N/mm}), \tag{4}$$

where ν is the Poisson's ratio, E_c is the elastic modulus.

The parameter of elastic-plastic failure (J_{Ic}) was calculated by using the area under the load versus deflection curve until the specimen rupture:

$$J_{Ic} = \frac{A}{2b(h - a_0)} \text{ (N/mm)}, \tag{5}$$

where A is the energy retained by the unit cross-sectional area in the beam sample until the peak load F_p is reached.

The crack tip opening displacement (CTOD) is another feature needed to evaluate the fracture toughness in the elastic-plastic region. The CTOD representation is the displacement at the primary tip of crack and the 90° intersection, and can be calculated as follows:

$$\text{CTOD} = \frac{6F_p a_0 l}{E_c b h^2} \text{V}_1(\alpha) \text{ (μm)}, \tag{6}$$

$$\text{V}_1(\alpha) = 0.76 - 2.28\alpha + 3.87\alpha^2 - 2.04\alpha^3 + \frac{0.66}{1 - \alpha^2} \tag{7}$$

The HPC brittleness could be determined by the characteristic length l_{ch}. The shorter the characteristic length, the more brittle the HPC is. Conversely, the greater the characteristic length, the more ductile the material is. The characteristic length is determined in accordance with the below equation [55]:

$$l_{ch} = \frac{E_c G_{Ic}}{f_t^2} \text{ (mm)}, \tag{8}$$

where f_t is the splitting tensile strength.

HPC flexural performance is critical for safeguarding infrastructure from severe weather conditions. The flexural strength of HPC containing CSF and its variability are given in Figure 8.

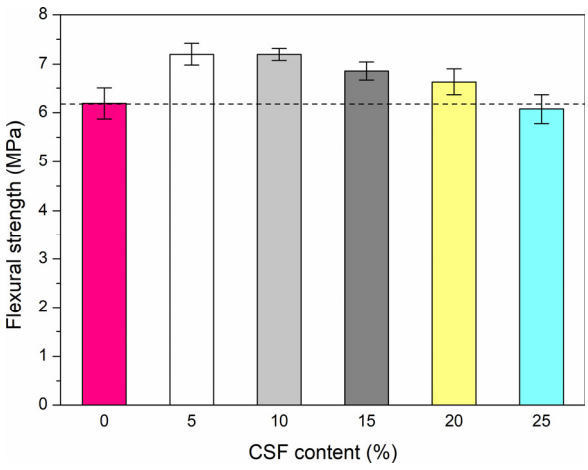

Figure 8. Differences in flexural strength with CSF substitution.

The replacement of cement by 5%, 10%, 15%, and 20% of the CSF content in HPC enhanced the flexural strength by 16%, 16%, 11%, and 7%, respectively, compared to reference specimens without CSF. However, strength decreased by 2% for 25% CSF content compared to control HPC. The average flexural strength increases from 0% to 10% and decreases from 10% to 25% of the CSF content. For HPC mixtures with a W/B ratio of 0.25, the compatibility between flexural and tensile splitting strength may affected by HPC brittleness. As will be exposed, the brittleness related to the characteristic length of HPC mixtures with a W/B ratio of 0.25 increases from 0% to 15% and decreases from 15% to 25%. This suggests a more fragile crack development, which may result in increased flexural strength. Wu et al. [3] found that the flexural strength increased by about 11%,

15%, 29%, and 18%, when 10%, 15%, 20%, and 25% silica fume were applied, respectively. Kansal et al. [56] stated that the substitution of fine aggregate with silica fume up to 10% in attendance of 2% nanosilica and 20% steel slag as a partial replacement of coarse aggregate exhibited the maximum flexural strength. It was found that the increase in the substitution of silica fume and steel slag above this value caused an insignificant decrease in the flexural strength. In addition, it was stated that the air holes were occupied by a greater content of silica fume and steel slag, and the reduced water availability may have limited the hydration reaction, adversely affecting the flexural strength of the concrete.

The average values of the HPCs fracture properties determined based on Equations (2)–(8) are given in Table 5.

Table 5. Average fracture characteristics of HPC with various CSF content.

Mixture ID	F_p (kN)	K_{Ic} (MN/m$^{1.5}$)	G_{Ic} (N/mm)	A (N × m)	J_{Ic} (N/mm)	CTOD (μm)	l_{ch} (mm)
CSF0	5.5	1.18	0.046	8.71	0.54	20.50	43.4
CSF5	6.4	1.37	0.060	9.66	0.60	23.13	42.2
CSF10	6.4	1.37	0.059	19.58	1.22	22.70	36.5
CSF15	6.1	1.31	0.055	29.20	1.83	21.83	35.7
CSF20	5.9	1.26	0.051	12.63	0.79	21.25	37.5
CSF25	5.4	1.16	0.045	6.91	0.43	20.17	36.8

Variations in fracture energy and characteristic length with CSF content are shown in Figure 9a,b, respectively. The fracture energy increased with the increase in the CSF content up to 5% and then gradually reduces. The use of CSF revealed an enhancement in fracture energy of approximately 30.5%, 28%, 19.5%, and 11%, respectively, compared to the reference specimen when it was 5%, 10%, 15%, and 20% of the applied CSF content. However, the fracture energy decreased by 2% for 25% CSF content in comparison with reference HPC. The higher fracture energy showed that more of it was needed to fracture the HPC, and thus HPC had better fracture characteristics. On the other hand, HPC had poor fracture properties with lower fracture energy. Consequently, variations in fracture energy also indicate that lower CSF content helps to improve fracture-related properties of HPC. Kjellsen et al. [14] described that the average fracture energy increased with increasing compressive strength. However, quite large scatters were obtained in the fracture energy results, and therefore any conclusions regarding the influence of strength and age are uncertain. Therefore, any possible impact of silica fume on fracture energy is not clear.

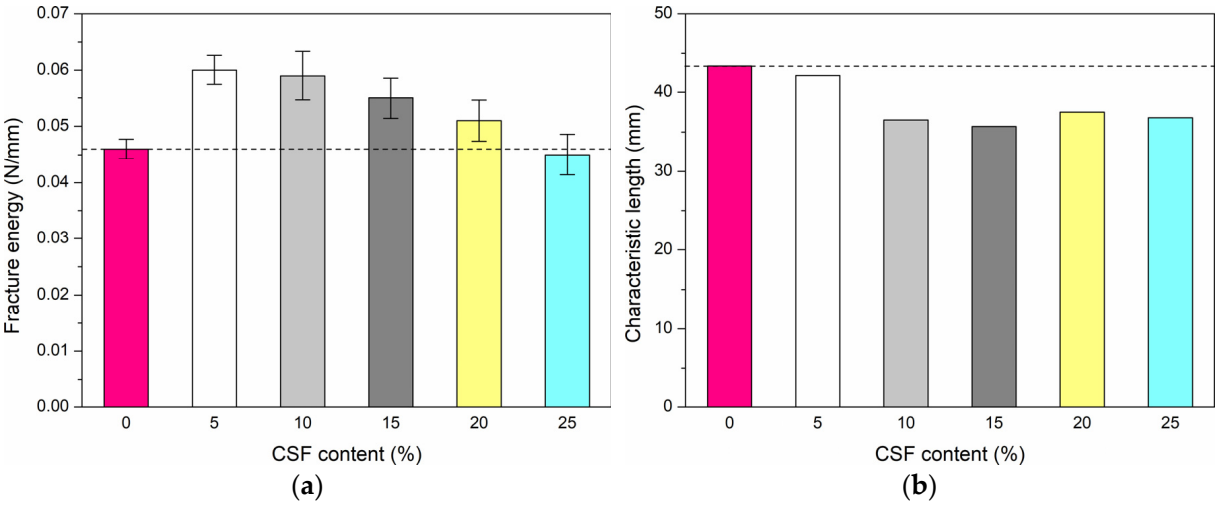

Figure 9. Differences in (**a**) fracture energy; (**b**) characteristic length with CSF content.

The characteristic length was determined based on average values of fracture energy, elastic modulus, and tensile splitting strength. The effect of the CSF content on the characteristic length was clear. It can be seen that there is a tendency for the characteristic length to decrease with growing compressive strength and CSF content (see Table 5 and Figure 9b). The results indicate that the CSF content of 5%, 10%, 15%, 20%, and 25% decreased the characteristic length by about 3%, 16%, 18%, 13.5%, and 15% in comparison with the reference HPC. Kjellsen et al. [14] informed that the addition of 10% silica fume increased the compressive strength by approximately 15%, while reducing the characteristic length by about 35%. A 50% increase in compressive strength is reached by decreasing the W/B ratio from 0.40 to 0.25, while the average reduction in characteristic length is approximately 25%.

The relationships for HPC between flexural strength and stress intensity factor, flexural strength and fracture energy, fracture energy and CTOD, compressive strength and characteristic length with and without CSF are displayed in Figure 10a–d, respectively.

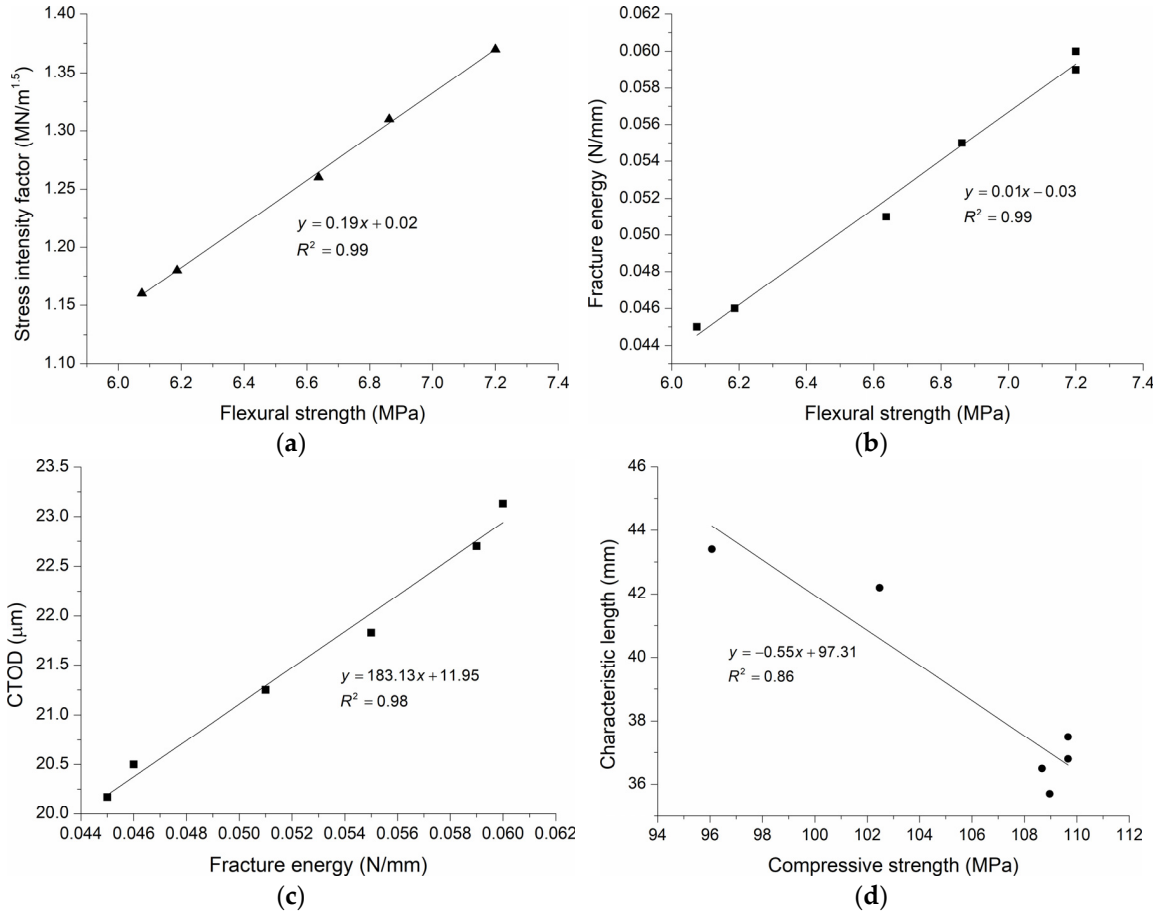

Figure 10. Correlation between (**a**) stress intensity factor and flexural strength; (**b**) fracture energy and flexural strength; (**c**) CTOD and fracture energy; (**d**) characteristic length and compressive strength, at 28 days.

These correlations demonstrate linearly enhancing stress intensity factor and fracture energy with increasing flexural strength, as well as linearly improving CTOD with increasing fracture energy for HPC specimens with and without CSF. On the other hand, the last correlation demonstrates a linearly decreasing characteristic length with the improvement of compressive strength. These correlations demonstrate strong R^2 values for the HPC specimens. The predicted equations for stress intensity factor, fracture energy, CTOD and characteristic length for HPC specimens with and without CSF are specified by:

$$K_{Ic} = 0.19 f_{t,fl} + 0.02 \quad (9)$$

$$G_{Ic} = 0.01 f_{t,fl} - 0.03 \quad (10)$$

$$CTOD = 183.13 G_{Ic} + 11.95 \quad (11)$$

$$l_{ch} = -0.55 f_c + 97.31 \quad (12)$$

3.5. Microstructure

The addition of condensed silica fume changes the chemical composition and properties of HPC. Figure 11 shows that as the content of CSF increases, the color of HPC becomes darker and the number and size of pores increases. This is due to a decrease in workability of HPC with an increase in the CSF substitution due to its high water demand and high specific surface area. Vikan and Justnes [50] observed that workability deteriorated, and higher viscosity caused the formation of air bubbles when the silica fume substitution surpassed a certain value. This can decrease the superiority of the HPC structure and the interfacial zone between its ingredients, and consequently decrease the compressive, tensile splitting, and flexural strength, as well as elastic modulus and fracture properties.

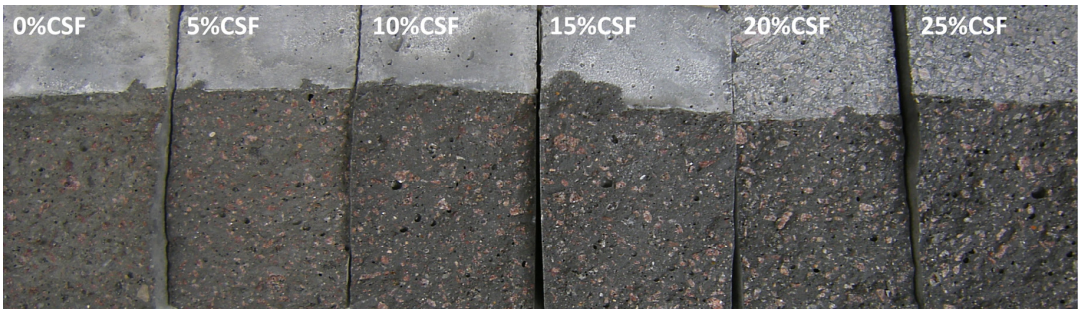

Figure 11. Split cross-sections of notched HPC beam specimens.

After testing the tensile splitting strength, 3 specimens of each HPC mixture were prepared for microstructure analysis. Using a scanning electron microscope (SEM), HPC micropores and microcracks were assessed depending on the CSF content. Figures 12 and 13 show images of all 6 HPC mixtures in 200× and from 4000× to 20,000× magnification, respectively.

CSF acts similarly to a binder to alter the structure of pores and form a dense HPC microstructure with a reduced amount of interfacial transition zone (ITZ). Because of this, HPC permeability is reduced. Thus, the solutions penetration containing harmful sulphates as well as has a chance to be meaningfully reduced.

The structure of the pores largely determines the durability and permeability of HPC. On the basis of the image analysis of several dozen microphotographs, it was found that the pore dimensions were in the range of 64–190 µm, 47–186 µm, 40–180 µm, 36–160 µm, 32–145 µm, 25–100 µm, for HPC with CSF content of 0%, 5%, 10%, 15%, 20%, and 25%, respectively. It was established that the pores number reduced with increasing CSF substitution. A reduction in macropores size was also found due to the CSF presence. The microstructure of HPC is improved due to the high pozzolanic activity of the CSF (in Figures 12 and 13). The binding activity is revealed by the CSH gel, which is formed as a result of the reaction of CSF with $Ca(OH)_2$ throughout hydration in an alkaline environment [19]. The resulting CSH gel fills holes and reduces the porosity of cementitious hydration products (see Figure 13). The CSH gel acts as a binder and provides a stronger bond between the aggregate grain and the paste. Consequently, it decreases the amount of free $Ca(OH)_2$, densifies ITZ, and finally increases HPC strength. $Ca(OH)_2$ reacts with CSF as it cannot hydrate directly with water [19]. The addition of CSF improves strength to a limited extent, but its higher amount, i.e., 25% content, and the lower amount of water in HPC may result in inhomogeneity of the mixture and low adhesion. Zhang Z. et al. [57] stated that due to the high pozzolanic activity, the porosity of the concrete is decreased, but the ITZ is improved through the consumption of calcium hydroxide and a marked increase in the number of hydration products. As previously mentioned, Vikan and Justnes [50]

stated that the addition of 15–20% silica fume decreased porosity and improved strength due to the pozzolanic reaction and filling effect. In contrast, 25% silica fume increased yield stress and plastic viscosity, which may result in the entrapment of additional air.

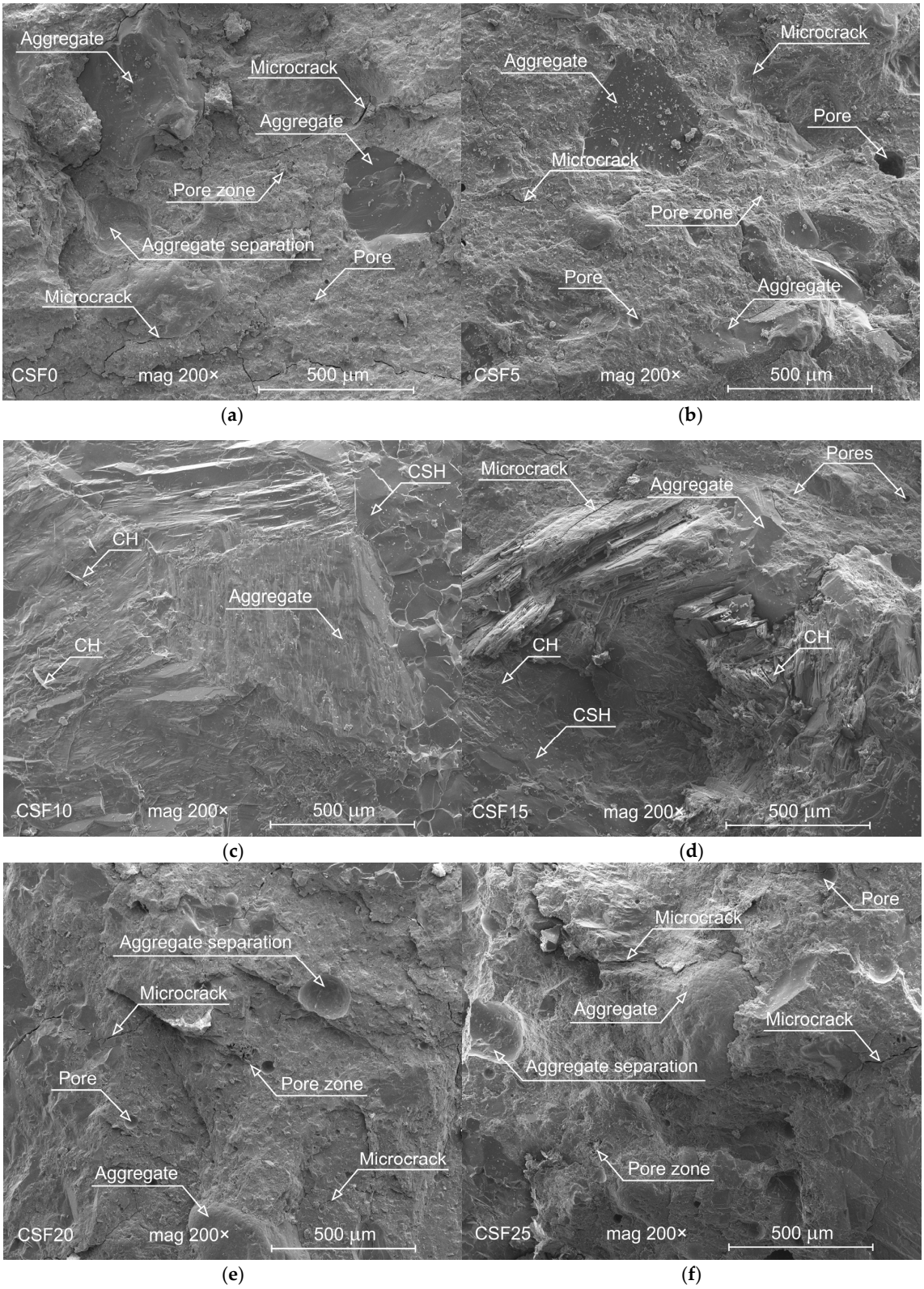

Figure 12. SEM microphotographs in 200× magnification for HPC with CSF content of (**a**) 0%; (**b**) 5%; (**c**) 10%; (**d**) 15%; (**e**) 20%; (**f**) 25%.

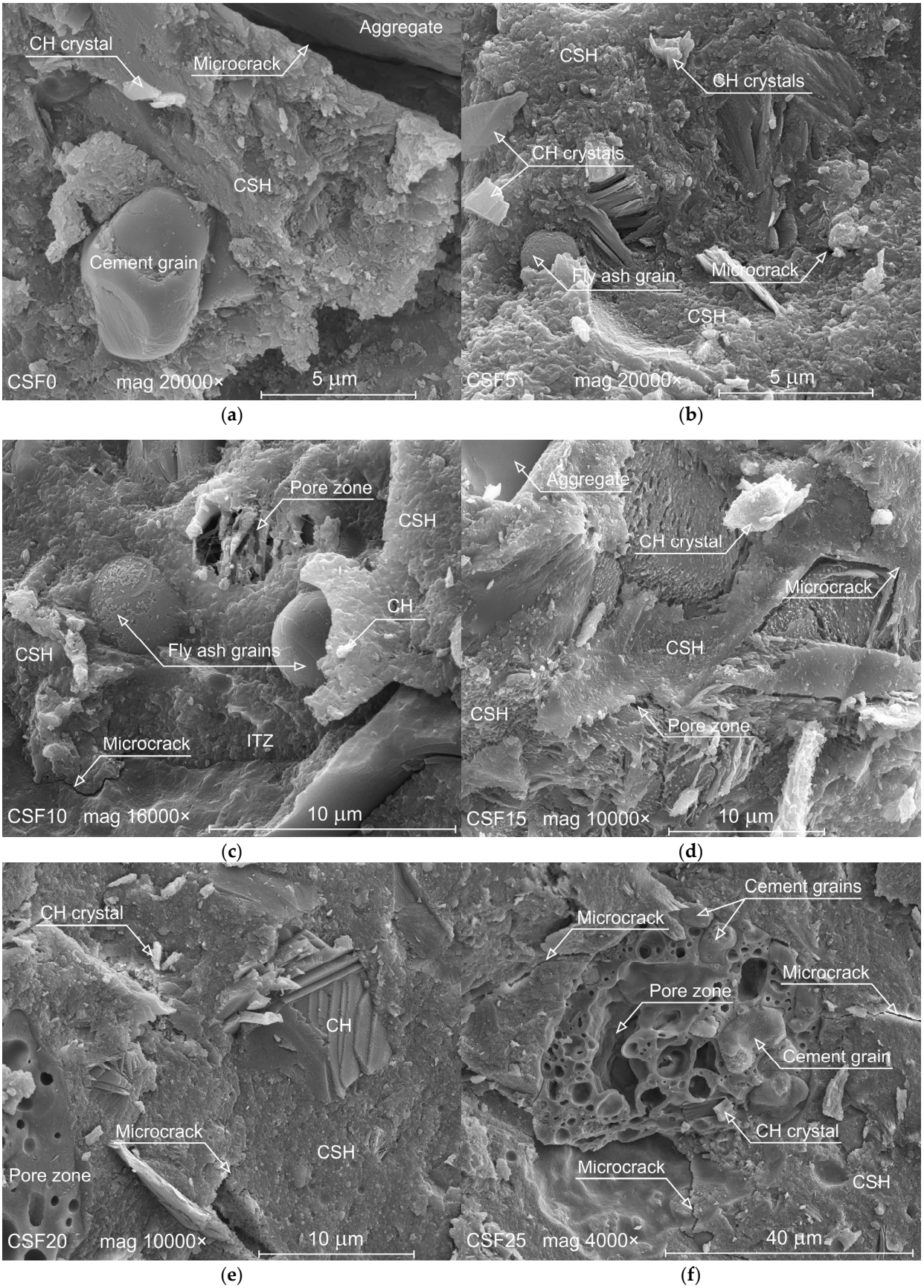

Figure 13. SEM microphotographs in magnification from 4000× to 20,000× for HPC with CSF content of (**a**) 0%; (**b**) 5%; (**c**) 10%; (**d**) 15%; (**e**) 20%; (**f**) 25%.

No ettringite crystals were observed on HPC microphotographs, regardless of the addition of CSF. The reason was probably too little water, which is necessary for the CSF pozzolanic reaction and the formation of ettringite. In HPC, regardless of the addition of CSF, there were no individual CSF gel particles, which can usually be located in normal concrete. The obtained HPC was characterized by a very dense structure, which, however, decreased slightly with greater CSF substitution. Calcium hydroxide $Ca(OH)_2$ appeared sporadically and took the form of small local crystals (see Figure 13). ITZ in concrete is a transitional phase between aggregate grains and hydrated cement slurry, which determines the final strength and durability [22]. The HPC microphotographs show that the dense structure of the paste is practically in contact with the edges of the aggregate grain. It can be concluded that CSF contributes to the disappearance of ITZ in HPC, while in ordinary concrete there is a $Ca(OH)_2$-rich porous region with a thickness of approximately 40–50 µm surrounding the aggregate grains. In this study, CSF10 and CSF15 also showed less non-hydrated cement and smaller pore areas in the boundary zones of the aggregate grain and in the dense paste structure compared to other HPCs mixes. Chandra and Berntsson [22] noticed that with the increase of the water-cement ratio in concrete with the addition of CSF, the ITZ thickness and the degree of orientation of calcium hydroxide crystals increased.

There are clear differences in the average microcrack width between the HPC specimens, as shown in the SEM microphotographs in Figure 14. The microcracks of CSF10 were smaller than those of the high condensed silica fume content. Besides, HPC with 25% CSF had a higher average microcrack in comparison with the control mixture. This means that in HPC with CSF substitution up to 20%, post-hydration structures of high strength were formed. It can also be noticed that there is a trend between the microcracks width and the fracture energy. Additionally, a high content of silica fume can considerably increase the possibility of microcracking caused by autogenous shrinkage, especially in the case of HPC with a high content of binder supplementary materials and a low W/B ratio, which can negatively affect the mechanical properties [58]. In general, autogenous shrinkage increases with increasing CSF substitution and can cause microcracks. In HPC, however, it may exert stresses at the boundary of the aggregate grain and cement paste, which, in turn, may lead to an increase in the bonding strength with the aggregate and reduction of cracks development. The formation of more high-strength hydration products, e.g., CSH, as well as the improvement of ITZ around the aggregate grains by minimizing or even eliminating it, resulted in narrower microcracks, which translated into greater stresses between the grains and the matrix, and improved bond strength to the aggregate.

Differences in the microcracks width depending on the CSF content are shown in Figure 15a. The average microcrack width decreased with increasing CSF substitution up to 10%. It was found that the HPC microcrack width regularly increases with the addition of CSF above 10%. The use of the CSF reduced the microcrack width by approximately 11%, 13%, 5.5%, and 2%, in comparison with the control specimen when 5%, 10%, 15%, and 20% CSF content was used, respectively. Nevertheless, the microcrack width increased by 2% for 25% CSF content in comparison with the reference HPC. This proves the effective reaction of CSF with CH and the formation of CSH, which reduced the width of microcracks and improved the bond strength in ITZ, as well as increasing matrix strength. Lee and Jacobsen [59] found that the poor quality of the bond between the aggregate and the cement slurry is mainly caused by a high concentration of pores and microcracks as well as the directional orientation of CH crystals and their high content. Wu et al. [3] found that ultra-high strength concrete with the addition of 15–25% SF was characterized by a higher CSH content, as well as lower porosity and CH content compared to the reference mix. In this study, 10% and 15% CSF substitutions were adequate to improve ITZ along with bond strength to aggregate grains and cement paste.

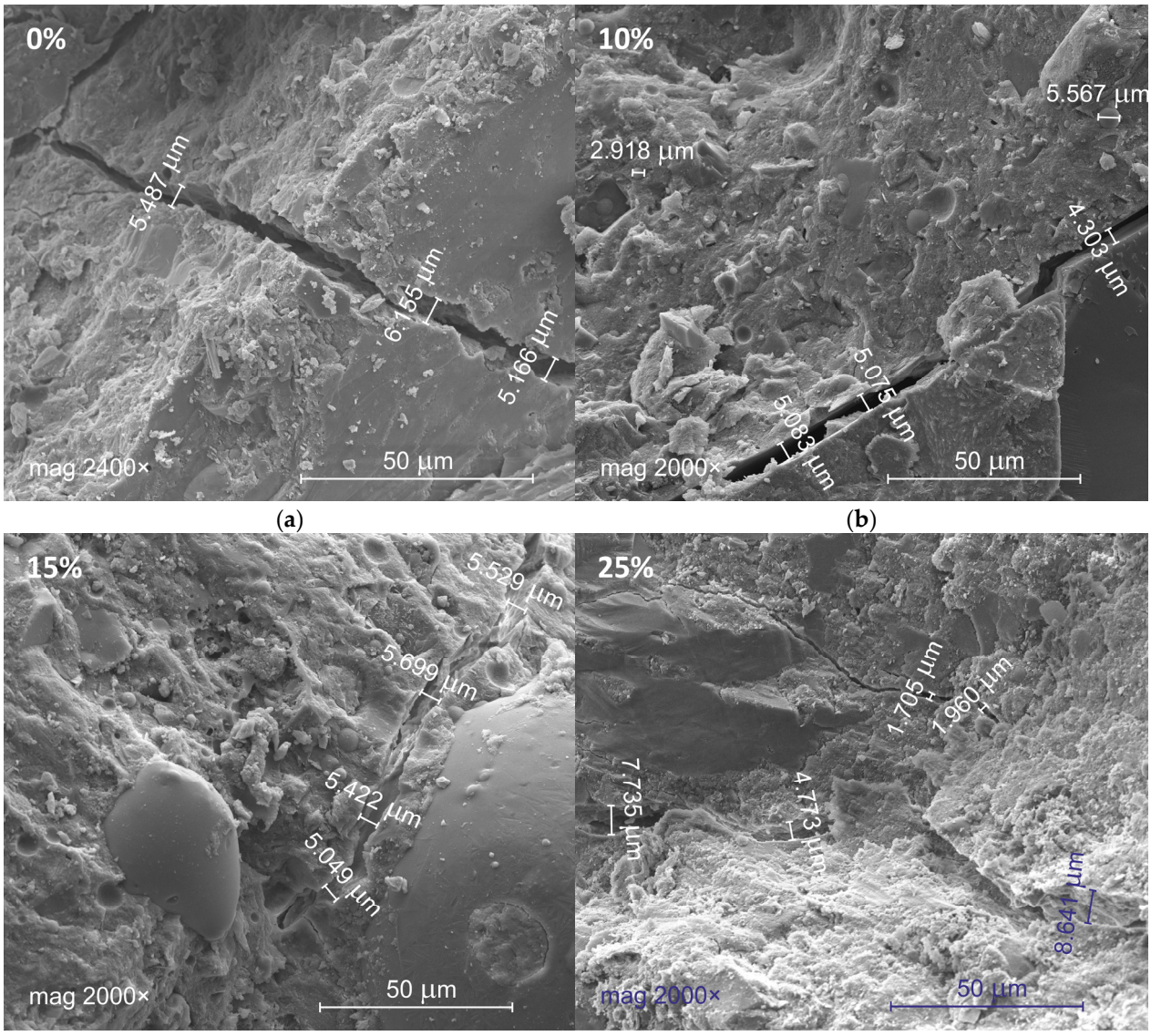

Figure 14. Differences in microcracks widths of HPC with CSF content of (**a**) 0%; (**b**) 10%; (**c**) 15%; (**d**) 25%.

The relationship for HPC between the microcrack width and the fracture energy without and with CSF is demonstrated in Figure 15b.

This correlation reveals linearly decreasing microcrack width with increasing fracture energy for HPC specimens with and without CSF. The correlation demonstrates strong R^2 values for the HPC specimens. The predicted equation of the microcrack width for HPC specimens with and without CSF is specified by:

$$w_m = 8.21 G_{Ic} - 52.19 \quad (13)$$

The above results show that the compressive strength, tensile split strength, elastic modulus, flexural strength, fracture properties, as well as the microstructure of HPC with changes in CSF replacement are closely related. Moreover, the addition of CSF can increase the CSH content and thus reduce microcracks and porosity due to the high SiO_2 content and ultra-fine particle size. The higher packing density of the supplemental cementitious material in the paste matrix reduced microcracks and porosity. For this reason, a higher content of CSH is necessary to obtain high mechanical properties.

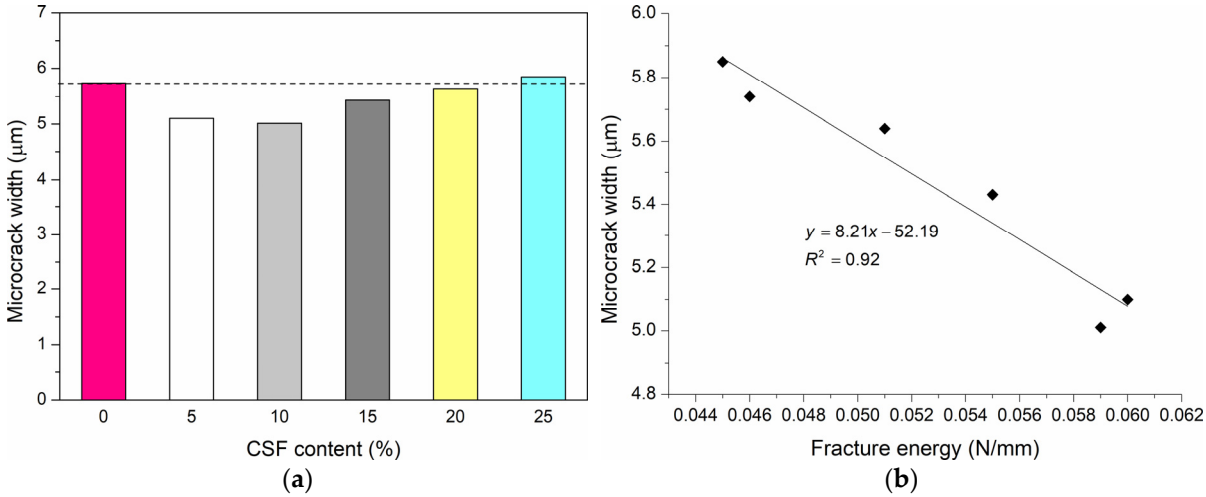

Figure 15. (**a**) Variation of microcrack width with SF content; (**b**) correlation between microcrack width and fracture energy after 28 days.

4. Conclusions

High performance concrete was studied for compressive strength, tensile splitting strength, elastic modulus, flexural strength, fracture properties, and microstructure. Six mixes of HPC containing condensed silica fume in the range of 0–25% as well as a water/binder ratio of 0.25 were tested. The specimens were maturated in water at 20 °C and examined after 28 days. On the basis of the results of these examinations, the following conclusions can be drawn:

- The compressive strength increases in the range of 6.5–14% with increasing CSF content compared to reference specimens without the implementation of CSF.
- The tensile splitting strength of HPC improves significantly with the addition of CSF. Tensile splitting strength increases in the range of 7–26% in comparison with the reference specimens. In the tested HPC, the values of the tensile splitting strength are in the range of 5.5–6.5% of the compressive strength, while for normal strength concrete this value is about 10%.
- The elastic modulus improves gradually as the CSF content increases to 10%, and then decreases to 25% CSF. It increases slightly in the range of 3–4.5% with the 5–20% addition of CSF, compared to the reference HPC. On the contrary, the modulus of elasticity is decreased by 0.5% for 25% CSF.
- Replacing the cement with 5–20% CSF in HPC significantly increases the flexural strength in the range of 7–16% compared to reference HPC. In contrast, for 25% CSF content, the flexural strength decreases by 2%.
- The 5–20% use of CSF significantly improves fracture energy in the range of 11–30.5% compared to reference HPC. However, the fracture energy decreases by 2% for 25% CSF.
- The characteristic length decreases in the range of 3–18% with the 5–25% addition of CSF, compared to the reference mix. HPC with 15% CSF substitution is the most brittle, which is due to the shortest characteristic length.
- The reduction of ITZ around the aggregate grains and the formation of higher-strength hydration products results in smaller microcrack widths in all CSF-added HPC.
- The microcrack width gradually decreases in the range of 11–2% with increasing CSF content from 5% to 20%, in comparison with the reference HPC. However, the microcrack width increases by 2% for 25% CSF.
- HPC containing CSF is characterized by a significant increase in compressive strength (up to 14% with 20% and 25% CSF) and flexural strength (16% with 5% and 10% CSF). However, the most significant improvements can be seen in splitting tensile strength (up to 26% with 10% CSF) and fracture energy (30.5% with 5% CSF). Significant de-

creases in the characteristic length (up to 18% with 15% CSF) and the width of the micro-cracks (13% with 10% CSF) are related to the greater brittleness and better durability of HPC concrete with the addition of CSF, respectively. In turn, the increase in modulus of elasticity is negligible (up to 4.5% with 10% CSF). Therefore, condensed silica fume can be used to produce high performance, sustainable concrete, but replacement should not exceed 20%.

Funding: This research received no external funding.

Institutional Review Board Statement: Not applicable.

Informed Consent Statement: Not applicable.

Data Availability Statement: The data that support the findings of this study are available from the corresponding author, P.S., upon reasonable request.

Acknowledgments: The author would like to thank the CEMEX Company for donating the materials for this study, as well as every person/department who helped throughout the research work. The careful review and constructive suggestions by the anonymous reviewers are graciously acknowledged.

Conflicts of Interest: The author declares no conflict of interest.

References

1. Meyer, C. The greening of the concrete industry. *Cem. Concr. Compos.* **2009**, *31*, 601–605. [CrossRef]
2. Seleem, H.E.-D.H.; Rashad, A.M.; El-Sabbagh, B.A. Durability and strength evaluation of high-performance concrete in marine structures. *Constr. Build. Mater.* **2010**, *24*, 878–884. [CrossRef]
3. Wu, Z.; Shi, C.; Khayat, K. Influence of silica fume content on microstructure development and bond to steel fiber in ultra-high strength cement-based materials (UHSC). *Cem. Concr. Compos.* **2016**, *71*, 97–109. [CrossRef]
4. Pedro, D.; de Brito, J.; Evangelista, L. Durability performance of high-performance concrete made with recycled aggregates, fly ash and densified silica fume. *Cem. Concr. Compos.* **2018**, *93*, 63–74. [CrossRef]
5. Smarzewski, P. Mechanical Properties of Ultra-High Performance Concrete with Partial Utilization of Waste Foundry Sand. *Buildings* **2020**, *10*, 11. [CrossRef]
6. Zhang, P.; Han, S.; Golewski, G.L.; Wang, X. Nanoparticle-reinforced building materials with applications in civil engineering. *Adv. Mech. Eng.* **2020**, *12*, 1–4. [CrossRef]
7. Brescia-Norambuena, L.; González, M.; Avudaiappan, S.; Saavedra Flores, E.I.; Grasley, Z. Improving concrete underground mining pavements performance through the synergic effect of silica fume, nanosilica, and polypropylene fibers. *Constr. Build. Mater.* **2021**, *285*, 122895. [CrossRef]
8. Smarzewski, P. Property Assessment of Self-compacting Basalt Fiber Reinforced Concrete. In *Fibre Reinforced Concrete: Improvements and Innovations II*; Serna, P., Llano-Torre, A., Martí-Vargas, J., Navarro-Gregori, J., Eds.; RILEM Book series; Springer: Cham, Switzerland, 2022; Volume 36, pp. 186–197. ISBN 978-3-030-83718-1. [CrossRef]
9. Khan, K.; Ahmad, W.; Amin, M.N.; Nazar, S. Nano-Silica-Modified Concrete: A Bibliographic Analysis and Comprehensive Review of Material Properties. *Nanomaterials* **2022**, *12*, 1989. [CrossRef]
10. Smarzewski, P.; Stolarski, A. Properties and Performance of Concrete Materials and Structures. *Crystals* **2022**, *12*, 1193. [CrossRef]
11. Yogendran, V.; Langan, B.W.; Haque, M.N.; Ward, M.A. Silica fume in high-strength concrete. *ACI Mater. J.* **1987**, *84*, 124–129.
12. Russell, H.G.; Chairman; Anderson, A.R.; Banning, J.O.; Cantor, I.G.; Carrasquillo, R.; Cook, J.E.; Frantz, G.; Hester, W.; Anderson, D.; et al. ACI, A. 363R-92, State-of-the-art report on high-strength concrete (reapproved in 1997). *Comput. Sci.* **1998**, *363*, 92.
13. Sabir, B.B. High-strength condensed silica fume concrete. *Mag. Concr. Res.* **1995**, *47*, 219–226. [CrossRef]
14. Kjellsen, K.O.; Hallgren, M.; Wallevik, O.H. Fracture mechanical properties of high-performance concrete—Influence of silica fume. *Mater. Struct.* **2000**, *33*, 552–558. [CrossRef]
15. Zhou, F.; Barr, B.; Lydon, F. Fracture properties of high strength concrete with varying silica fume content and aggregates. *Cem. Concr. Res.* **1995**, *25*, 543–552. [CrossRef]
16. Tasdemir, C.; Tasdemir, M.A.; Lydon, F.D.; Barr, B.I. Effects of silica fume and aggregate size on the brittleness of concrete. *Cem. Concr. Res.* **1996**, *26*, 63–68. [CrossRef]
17. Köksal, F.; Altun, F.; Yiğit, I.; Şahin, Y. Combined effect of silica fume and steel fiber on the mechanical properties of high strength concretes. *Constr. Build. Mater.* **2008**, *22*, 1874–1880. [CrossRef]
18. Smarzewski, P. Comparative Fracture Properties of Four Fibre Reinforced High Performance Cementitious Composites. *Materials* **2020**, *13*, 2612. [CrossRef]
19. Khan, M.; Rehman, A.; Ali, M. Efficiency of silica-fume content in plain and natural fiber reinforced concrete for concrete road. *Constr. Build. Mater.* **2020**, *244*, 118382. [CrossRef]

20. Smarzewski, P. Flexural toughness evaluation of basalt fibre reinforced HPC beams with and without initial notch. *Compos. Struct.* **2019**, *235*, 111769. [CrossRef]
21. Ibrahim, Y.E.; Adamu, M.; Marouf, M.L.; Ahmed, O.S.; Drmosh, Q.A.; Malik, M.A. Mechanical Performance of Date-Palm-Fiber-Reinforced Concrete Containing Silica Fume. *Buildings* **2022**, *12*, 1642. [CrossRef]
22. Chandra, S.; Berntsson, L. Use of Silica Fume in Concrete. In *Waste Materials Used in Concrete Manufacturing*; Chandra, S., Ed.; Noyes Publications: Westwood, NJ, USA, 1997; p. 669.
23. Smarzewski, P. Influence of silica fume on mechanical and fracture properties of high performance concrete. *Procedia Struct. Integr.* **2019**, *17*, 5–12. [CrossRef]
24. Gupta, S. Application of Silica Fume and Nanosilica in Cement and Concrete–A Review. *J. Today's Ideas -Tomorrow's Technol.* **2013**, *1*, 85–98. [CrossRef]
25. Hooton, R.D. Influence of silica fume replacement of cement on physical properties and resistance to sulfate attack, freezing and thawing, and alkali-silica reactivity. *ACI Mater. J.* **1993**, *90*, 143–151.
26. Siddique, R.; Chahal, N. Use of silicon and ferrosilicon industry by-products (silica fume) in cement paste and mortar. *Resour. Conserv. Recycl.* **2011**, *55*, 739–744. [CrossRef]
27. Lazaro, A.; Yu, Q.; Brouwers, H. Nanotechnologies for sustainable construction. *Sustain. Constr. Mater.* **2016**, *4*, 55–78. [CrossRef]
28. Dybeł, P.; Furtak, K. Influence of silica fume content on the quality of bond conditions in high-performance concrete specimens. *Arch. Civ. Mech. Eng.* **2017**, *17*, 795–805. [CrossRef]
29. Zhang, Y.; Zhang, W.; Zhang, Y. Combined effect of fine aggregate and silica fume on properties of Portland cement pervious concrete. *Adv. Concrete Constr.* **2019**, *8*, 47–54.
30. Yin, X.; Sun, H.; Zeng, W.; Xiang, Y.; Zhou, T.; Ma, D.; Yang, C. Manipulating the LUMO distribution of quinoxaline-containing architectures to design electron transport materials: Efficient blue phosphorescent organic light-emitting diodes. *Org. Electron.* **2020**, *37*, 439–447. [CrossRef]
31. Toutanji, A.H.; Bayasi, Z. Effect of curing procedures on properties of silica fume concrete. *Cem. Concr. Res.* **1999**, *29*, 497–501. [CrossRef]
32. Atis, C.; Özcan, F.; Kılıç, A.; Karahan, O.; Bilim, C.; Severcan, M. Influence of dry and wet curing conditions on compressive strength of silica fume concrete. *Build. Environ.* **2005**, *40*, 1678–1683. [CrossRef]
33. Kjellsen, K.O.; Wallevik, O.H.; Fjällberg, L. Microstructure and microchemistry of the paste–aggregate interracial transition zone of high-performance concrete. *Adv. Cem. Res.* **1998**, *10*, 33–40. [CrossRef]
34. Wedding, P.A.; Swamy, R.N. Properties of high-strength concrete. *Cem. Concr. Aggreg.* **1986**, *8*, 33–41. [CrossRef]
35. John, R.; Shah, S.P. Fracture Mechanics Analysis of High-Strength Concrete. *J. Mater. Civ. Eng.* **1989**, *1*, 185–198. [CrossRef]
36. Ahmad, S.H.; Shah, S.P. Complete triaxial stress–strain curves for concrete. *Proc. Am. Soc. Civ. Eng.* **1982**, *108*, 728–742. [CrossRef]
37. Kadri, E.H.; Duval, R.; Aggoun, S.; Kenai, S. Silica fume effect on hydration heat and compressive strength of high-performance concrete. *ACI Mater. J.* **2009**, *106*, 107.
38. Gesoglu, M.; Güneyisi, E.; Asaad, D.; Muhyaddin, G. Properties of low binder ultra-high performance cementitious composites: Comparison of nanosilica and microsilica. *Constr. Build. Mater.* **2016**, *102*, 706–713. [CrossRef]
39. Li, L.; Zheng, J.; Ng, P.; Zhu, J.; Kwan, A. Cementing efficiencies and synergistic roles of silica fume and nano-silica in sulphate and chloride resistance of concrete. *Constr. Build. Mater.* **2019**, *223*, 965–975. [CrossRef]
40. Duval, R.; Kadri, E. Influence of Silica Fume on the Workability and the Compressive Strength of High-Performance Concretes. *Cem. Concr. Res.* **1998**, *28*, 533–547. [CrossRef]
41. Toutanji, H.A.; El-Korchi, T. The influence of silica fume on the compressive strength of cement paste and mortar. *Cem. Concr. Res.* **1995**, *25*, 1591–1602. [CrossRef]
42. Zhang, P.; Liu, C.H.; Li, Q.F.; Zhang, T.H.; Wang, P. Fracture properties of steel fibre reinforced high-performance concrete containing nano-SiO2 and fly ash. *Curr Sci.* **2014**, *106*, 980–987.
43. Smarzewski, P. Influence of basalt-polypropylene fibres on fracture properties of high performance concrete. *Compos. Struct.* **2018**, *209*, 23–33. [CrossRef]
44. Smarzewski, P. Study of Bond Strength of Steel Bars in Basalt Fibre Reinforced High Performance Concrete. *Crystals* **2020**, *10*, 436. [CrossRef]
45. Ahmad, W.; Khan, M.; Smarzewski, P. Effect of Short Fiber Reinforcements on Fracture Performance of Cement-Based Materials: A Systematic Review Approach. *Materials* **2021**, *14*, 1745. [CrossRef] [PubMed]
46. *PN-B-19707:2013-10*; Cement. Special Cement. Composition, Specifications and Conformity Criteria. 2013. Available online: https://sklep.pkn.pl/pn-b-19707-2013-10p.html?options=cart (accessed on 8 February 2023).
47. *PN-EN 197-1:2012*; Cement. Composition, Specifications and Conformity Criteria for Common Cements. 2012. Available online: https://sklep.pkn.pl/pn-en-197-1-2012p.html?options=cart (accessed on 8 February 2023).
48. *PN-EN 933-1:2012*; Tests for Geometrical Properties of Aggregates. Determination of Particle Size Distribution. Sieving Method. 2012. Available online: https://sklep.pkn.pl/pn-en-933-1-2012e.html?options=cart (accessed on 8 February 2023).
49. *PN-EN 12390-3:2019-07*; Testing Hardened Concrete. Compressive Strength of Test Specimens. 2019. Available online: https://sklep.pkn.pl/pn-en-12390-3-2019-07p.html?options=cart (accessed on 8 February 2023).
50. Vikan, H.; Justnes, H. Rheology of cementitious paste with silica fume or limestone. *Cem. Concr. Res.* **2007**, *37*, 1512–1517. [CrossRef]

51. *PN-EN 12390-6:2011*; Testing Hardened Concrete. Tensile Splitting Strength of Test Specimens. 2011. Available online: https://sklep.pkn.pl/pn-en-12390-6-2011p.html?options=cart (accessed on 8 February 2023).
52. *ASTM C469/C469M-14*; Standard Test Method for Static Modulus of Elasticity and Poisson's Ratio of Concrete in Compression. ASTM International: West Conshohocken, PA, USA, 2014.
53. RILEM TC 89-FMT. Size-effect method for determining fracture energy and process zone size of concrete. *Mat. Struct.* **1990**, *23*, 461–465. [CrossRef]
54. Gettu, R.; Shah, S.P. Fracture mechanics. In *High Performance Concretes and Applications*; Shah, S.P., Ahmad, S.H., Eds.; Edward Arnold: London, UK, 1994; p. 337.
55. Montgomery, D.C. *Design and Analysis of Experiments*, 2nd ed.; John Wiley & Sons: New York, NY, USA, 1984.
56. Kansal, C.M.; Singla, S.; Garg, R. Effect of Silica Fume & Steel Slag on Nano-silica based High-Performance Concrete. *IOP Conf. Series: Mater. Sci. Eng.* **2020**, *961*, 012012. [CrossRef]
57. Zhang, Z.; Zhang, B.; Yan, P. Hydration and microstructures of concrete containing raw or densified silica fume at different curing temperatures. *Constr. Build. Mater.* **2016**, *121*, 483–490. [CrossRef]
58. Lura, P.; Jensen, O.; Breugel, K. Autogenous shrinkage in high-performance cement paste: An evaluation of basic mechanisms. *Cem. Concr. Res.* **2003**, *33*, 223–232. [CrossRef]
59. Lee, S.F.; Jacobsen, S. Study of interfacial microstructure, fracture energy, compressive energy and debonding load of steel fiber-reinforced mortar. *Mater. Struct.* **2011**, *44*, 1451–1465. [CrossRef]